Original Research Article

LncRNA APTR amplification serves as a potential glioma biomarker and promotes glioma progression via miR-6734-5p/ TCF7/LEF1 axis

Heng Chen [a,b,c,1], Mengzhen Huang [a,b,c,1], Jiayi Li [a,b,c], Shanshan Zhang [d], Cuiyun Sun [e], Wenjun Luo [e], Lin Yu [a,b,c,*]

[a] *Department of Biochemistry and Molecular Biology, School of Basic Medical Sciences, Tianjin Medical University, Tianjin, 300070, China*
[b] *Laboratory of Molecular Immunology, Research Center of Basic Medical Science, Tianjin Medical University, Tianjin, 300070, China*
[c] *Tianjin Key Laboratory of Cellular and Molecular Immunology and Key Laboratory of the Educational Ministry of China, Tianjin Medical University, Tianjin, 300070, China*
[d] *Department of Radiology, Tianjin Medical University General Hospital, Tianjin, China*
[e] *Department of Neuropathology, Tianjin Key Laboratory of Injuries, Variations and Regeneration of the Nervous System, Key Laboratory of Post-trauma Neuro-repair and Regeneration in Central Nervous System of Education Ministry, Tianjin Neurological Institute, Tianjin Medical University General Hospital, Tianjin, China*

ABSTRACT

Background: Alu-mediated p21 transcriptional regulator (*APTR*) overexpression is detected in different human cancers; however, few reports have investigated *APTR* gene amplification conditions. Furthermore, whether *APTR* amplification is related to glioma malignancy and the underlying mechanism remain unknown.
Methods: *APTR* amplification and expression levels in 153 glioma samples were analyzed using qPCR. Correlations between APTR and patient prognosis were evaluated using Kaplan-Meier survival and COX regression analyses. Both *in vitro* and *in vivo* phenotypic assays were performed to confirm the carcinogenic effects of APTR in glioblastoma (GBM) cells. RNA-sequencing and RNA immunoprecipitation and luciferase reporter assays were performed to confirm APTR as a competing endogenous RNA (ceRNA) and to identify the downstream axis of APTR.
Results: Our results suggest that *APTR* amplification and overexpression are novel independent diagnostic biomarkers for predicting poor prognosis in patients with gliomas. APTR knockdown significantly repressed the proliferation and invasion of GBM cells, both *in vitro* and *in vivo*. APTR was demonstrated to absorb miR-6734-5p and upregulate TCF7 and LEF1 expression. Taken together, these results suggest that APTR promotes the malignant phenotypes of GBM by inducing TCF7 and LEF1 expression.
Conclusion: We identified APTR as a novel prognostic biomarker in patients with gliomas and confirmed that APTR is a ceRNA that promotes glioma progression via the APTR/miR-6734-5p/TCF7/LEF1 axis.

1. Introduction

The morbidity rate of gliomas is the highest among primary intracranial tumors [1]. Among glioma types, World Health Organization (WHO) grade 4 glioblastoma (GBM) has the highest incidence and an extremely poor prognosis [2]. Although traditional treatment methods such as surgical resection followed by temozolomide chemotherapy are widely applied, patients still suffer from a high risk of recurrence and have low survival rates owing to the invasiveness of GBM [3]. New biomarkers for glioma diagnosis are urgently needed. Glioma cell genomes are prone to rearrangement, leading to abnormal variations in the copy numbers of key genes [4]. The copy number abnormalities in the aforementioned genes have a significant impact on GBM progression and patient prognosis [5]. Accumulated evidence from our own studies and previously reported results has confirmed that the amplification of EGFR [6], GATAD1 [7] and other key onco-potential genes [8] induce malignant GBM phenotypes and predict poor outcomes in patients with GBM.

In this study, we analyzed the amplification of Alu-mediated p21 transcriptional regulator gene (*APTR*) and found that its copy number

and expression level were positively associated with WHO grade and glioma malignancy. Furthermore, both *APTR* amplification and over-expression can be reliably quantified using high-sensitivity assays (e.g., qPCR), underscoring their potential as molecular biomarkers for glioma stratification and prognostic prediction.

APTR is located on chromosome 7q11.23 and its transcription product (APTR) is a long noncoding RNA. Few studies have addressed the functions of APTR. APTR was initially identified as a transcription repressor of p21 [9]; however, it may also participate in estrogen signal transduction by binding to the estrogen receptor (ER) [10]. Additional evidence has confirmed that APTR can regulate YAP1 levels via inter-action with mir-132–3p, which suggests the competing endogenous RNA (ceRNA) potential of APTR [11]. Hence, the detailed molecular func-tions of APTR need to be clarified. Recent studies have shown that abnormal APTR expression occurs in different tissues such as liver cirrhosis [12], gastric cancer [13], thyroid cancer [14] and osteosar-coma [11]. However, larger, well-annotated glioma sample sets are still needed to ascertain the subclassification biomarker potential of APTR.

The Wnt signaling pathway influences the invasiveness, drug resis-tance, and angiogenesis of GBM cells, and is a focal point in glioma research [15]. Active classical Wnt signaling prompts members of the T-cell factor/lymphoid enhancer factor (TCF/LEF) family to recruit β-catenin to the DNA region, thus initiating the transcriptional activa-tion of TCF target genes. Wnt-induced transcriptional activation is mediated exclusively by TCF/LEF [16]. Many studies mainly focus on the roles played by TCF7/LEF1 in the Wnt/β-catenin signaling pathway.

We identified *APTR* copy number amplification and overexpression in glioma tissues. These alterations positively correlate with tumor grade and predict poorer prognosis, highlighting their potential as biomarkers for glioma stratification. Mechanistically, we confirmed that APTR functions as a ceRNA and binds to miR-6734-5p, which sequentially upregulates TCF7/LEF1 and promotes GBM progression.

2. Materials and methods

2.1. The clinical feature of tissue samples

A total of 153 glioma samples were obtained from the Tianjin Medical University General Hospital (TMUGH) (Supplementary Table 1). All patients with gliomas signed consent forms after being officially informed of the study. The diagnoses presented for the afore-mentioned samples were graded according to the WHO glioma classifi-cation by two separate pathologists. The TMUGH Ethics Committee verified that all procedures involving patient data adhered to the ethical principles of the Declaration of Helsinki (see ethics approval and consent to participate). The Cancer Genome Atlas (TCGA) (https://cancerge nome.nih.gov/) low-grade glioma (LGG) and glioblastoma (GBM) datasets were used to analyze *APTR* copy number, expression, and clinical features.

2.2. Copy number variation assay

The *APTR* copy number was detected using the TaqMan Copy Number Assay kit (assay ID: Hs04995058_cn, Hs04965917_cn, Thermo Fisher Scientific, Waltham, MA, USA). TaqMan Copy Number Reference RNase P was used as an internal reference (Thermo Fisher Scientific). Finally, the relative quantitative results were analyzed using Copy Caller software (Applied Biosystems, Waltham, MA, USA).

2.3. Immunohistochemistry (IHC)

Formalin-fixed, paraffin-embedded (FFPE) tissues were incubated with primary antibodies against TCF7 (1:500; Abcam, Cambridge, UK) and LEF1 (1:500; Abcam) (Supplementary Table 3). Protein visualiza-tion was achieved using the Vectastain ABC (Avidin-Biotin Complex) Detection System, which included the biotinylated secondary antibody

and ABC complex. Subsequently, 10 representative fields of view (400 ×) within high-expression hotspots were selected for analysis under a Leica DM6000B microscope. Quantitative assessment was performed using Image ProPlus 5.0 software (Media Cybernetics), where both positive cells and total cell counts were recorded across all 10 fields. The labeling index (LI [%]) was calculated as the percentage of positive cells relative to the total cellular population.

2.4. Cell culture and stable cell construction

U87MG and HEK293T cells were purchased from the American Type Culture Collection (Manassas, VA, USA). U251 cells were acquired from the National Biomedical Cell Line Resource (Beijing, China). The cell cultures were maintained at 37 °C under 5 % CO$_2$. The cells were incubated in Dulbecco's Modified Eagle's medium (DMEM) supple-mented with 10 % fetal bovine serum (BioInd, Shanghai, China). My-coplasma contamination was detected and prevented using qPCR (TransGen, Beijing, China).

The PGL3-basic plasmid (Promega, Madison, WI, USA) was modified by separately inserting the 7 × TCAAAG recognition sequence for TCF7 and the 5 × CCTTTGAA recognition sequence for LEF1, and was co-transfected with the pRL-TK Renilla luciferase plasmid (Promega) as a control to detect TCF and LEF1 activation levels within the Wnt signaling pathway. The pmirGLO micro RNA (miRNA) target plasmid (Promega) was specifically designed to assess miRNA activity by inserting target sequences. The pmirGlO-APTR, pmirGlO-TCF7 3′UTR, and pmirGlO-LEF 3′UTR were synthesized by GENEWIZ (Suzhou, China) based on the sequences provided. Lentiviral system package plasmids psPAX2 and pMD2.G were purchased from Addgene (Watertown, MA, USA). The pLKO.1 plasmid was acquired from Sigma-Aldrich (St. Louis, MA, USA), and the inserted shRNA sequences were synthesized by GENEWIZ. The three shRNA sequences included two APTR targeting shRNA (APTR-sh1, sense sequence: 5′-CCACTGTCGCTGGCGTGAA-3′ and APTR-sh2, sense sequence: 5′-CCAGGTACTGCCTTCTAAC-3′), and one control RNA (Scramble sequence: 5′-CCTAAGGTTAAGTCGCCCTCG-3′).

U87MG and U251 wild-type cells were infected with the lentivirus. After 48 h of infection, cells were treated with 1.4 μg/mL puromycin (Solarbio, Beijing, China) in cycles of three days for two weeks until stable APTR knockdown cell lines were selected. These cell lines were subsequently named U87-sh1, U87-sh2, U87-Scamble, U251-sh1, U251-sh2, and U251-Scamble. For lentivirus package, 293T cells were trans-fected with polyethylenimine (PEI) transfection reagent (MedChemEx-press, Monmouth Junction, NJ, USA).

2.5. miRNA mimics and antisense oligonucleotide

The miRNA oligonucleotides were obtained from GenePharma (Suzhou, China). Double-stranded microRNA mimics (Supplementary Table 2) including miR-151b mimics (sense sequence: 5′-UCGAGGAG-CUCACAGUCU-3′), miR-6734-5p mimics (sense sequence: 5′-UUGAGGGGAGAAUGAGGUGGAGA-3′), and mimic control (sense sequence: 5′-UUCUCCGAACGUGUCACGUTT-3′).

The miRNA inhibitors (Supplementary Table 2) used were single-stranded antisense oligonucleotide molecules (ASO), including miR-6734-5p inhibitor (sequence: 5′-UCUCCACCUCAUUCUCCCCUCAA-3′) and inhibitor control (sequence: 5′-CAGUACUUUUGUGUAGUACAA-3′).

2.6. Transwell assay

U87MG and U251 cells were seeded in hanging inserts with an 8-μm pore size at a density of 1×10^5 cells/well (Labselect, Beijing, China) in wells prepared with Matrigel (Corning, NY, USA). After 12–16 h, the cells had invaded the membrane. The inserts were removed and fixed in 4 % paraformaldehyde. Next, 0.2 % crystal violet (Solarbio, Beijing, China) was used to stain the cells, which were then allowed to dry. For

each insert, the mean number of invading cells was calculated from five individual fields.

2.7. Wound healing assay

GBM cells were seeded in 6-well plates at a density of 9×10^5 cells/well. Each well contained three evenly scratched parallel cell lines. The healing area was observed using an inverted microscope (Olympus, Tokyo, Japan) at $10 \times$ magnification, and images were taken at 0, 9, and 24 h and analyzed using ImageJ (NIH, Bethesda, MD, USA, version 1.54b).

2.8. Cell proliferation assay

GBM cells were cultured in 96-well plates at a density of 1×10 cells/well for 8 h. The day of cell attachment was regarded as day 1, and proliferation was assessed on days 2–5. Cell proliferation was detected using the Cell Counting Kit-8 (CCK-8; Dojindo, Tabaru, Japan) according to the manufacturer's instructions. After incubation for 1.5 h, the optical density (OD) at 490 nm was quantified using a microplate spectrophotometer (Agilent Technologies, Santa Clara, CA, USA).

GBM cells were cultured in 6-well plates at a density of 1×10^3 cells per well for approximately one week. Cells were fixed with 4 % paraformaldehyde, stained with 0.4 % crystal violet (Solarbio), and allowed to dry. Colonies containing more than 50 cells were counted and images were captured. The average clone number of the three replicate wells was used to calculate the clone formation rate, which was calculated as the average number of clones divided by the number of inoculated cells.

2.9. Total RNA purification and qRT-PCR

Primers were synthesized by GENEWIZ (Supplementary Table 2). Total RNA was extracted using TRIzol (Vazyme, Nanjing, China), and the StarScript III All-in-one RT Mix (Genstar, Beijing, China) was used to synthesize cDNA. The miRNA 1st Strand cDNA Synthesis Kit (Vazyme) was used to produce miRNAs. The Fast SYBR qPCR Mix (Genstar) were used to perform qPCR on StepOne Real-Time PCR System (Thermo Fisher Scientific). GAPDH and U6 were used as the reference genes. The PCR program was set to 95 °C for 30 s and 60 °C for 1 min, and this was repeated for 40 cycles.

2.10. Cytoplasmic and nuclear RNA purification assay

RNA was isolated from 5×10^5 GBM cells using a Cytoplasmic and Nuclear RNA Purification Kit (Norgen Biotek, Thorold, Ontario, Canada). Subsequently, reverse transcription was performed using the StarScript III All-in-one RT Mix (Genstar). cDNA was amplified using APTR primers and electrophoresed on 3 % formaldehyde agarose gels for visualization. U6 and 18sRNA were amplified as the controls. The PCR reaction was performed 94 °C for 2 min and 60 °C for 30 s for 40 cycles.

2.11. Western blotting

Total protein was extracted from the cell lines using RIPA solution (Solarbio). Its concentration was determined using a bicinchoninic acid assay (Thermo Fisher Scientific). For SDS-PAGE gel electrophoresis, 20 µg of protein was loaded into each lane. The following antibodies (Supplementary Table 3) were used for detection: rabbit antibodies against LEF1 (1:500; Abcam), TCF7 (1:1000; Abcam), c-Myc (1:1000; Abcam), CCND1 (1:1000; Abcam), and GAPDH (1:10000; Abcam); and a mouse antibody against α-tubulin (1:10000; Abcam).

2.12. Fluorescence in situ hybridization

Fluorescein amidites (FAM)-labeled APTR DNA probe (sequence: 5′-

CCGCCGAGCTCTGACCTCCGAA-3′), negative control FAM-labeled scramble DNA probe and positive control FAM-labeled U6 DNA probe were synthesized by GENEWIZ (Supplementary Table 2). U87MG and U251 cells were seeded onto coverslips at a growth density of approximately 70 %. The cells were sequentially fixed, stained, and hybridized at 37 °C overnight. The dilution ration of probes was 1:100. The slides were then sealed using Fluoroshield mounting solution (Thermo Fisher Scientific). Images were captured using a DMI6000B fluorescence microscope (Leica, Wetzlar, Germany).

2.13. Luciferase reporter assay

Lipofectamine 3000 transfection reagent (Thermo Fisher Scientific) was used to transfect U87MG and U251 cells for 3′UTR luciferase reporter assay. While transfecting miRNA mimics, pmirGlO-APTR (wild type [WT] or mutant [MUT]), pmirGlO-TCF7-3′UTR (WT or MUT), and pmirGlO-LEF1-3′UTR (WT or MUT) was also transfected. The pGL3-basic and pRL-TK plasmids were transfected into GBM cells by Lipofectamine 3000, including control (Scramble) and APTR knockdown groups (APTR-sh1 and APTR-sh2). Using a GloMax Navigator Microplate Luminometer (Promega), reporter gene fluorescence units were quantified using a Luc-Pair Duo-Luciferase Assay Kit (GeneCopoeia, Rockville, MD, USA).

The TCF/LEF luciferase reporter plasmid (Hanbio, Shanghai, China) and Renilla plasmid (Promega) were cotransfected into U87MG and U251 cells using Lipofectamine 3000 (Thermo Fisher Scientific) according to the manufacturer's instructions. After 24 h, the cells were collected, and luciferase activity was assayed using the Dual-Luciferase Reporter Gene Assay Kit (Beyotime, Shanghai, China).

2.14. RNA immunoprecipitation (RIP) assay

The RIP assay was performed using an Imprint® RNA Immunoprecipitation kit (Sigma-Aldrich) in both U87MG and U251 cells using an AGO2 antibody (Abcam) and anti-IgG antibody. The precipitated RNA was obtained for cDNA synthesis and analyzed using qRT-PCR.

2.15. GBM cell line orthotopic xenograft

When the U87MG cell density reached approximately 60–70 % in 6-well plates, 1 mL of serum-free DMEM was added to each well. Each well was then transfected with 10 µL of 3.5×10^8 TU/mL CON101 (Ubi-MCS-firefly-Luciferase-IRES-Puromycin) lentivirus (GENE) and 40 µL of $25 \times$ HiTransG infection reagent. Seventy-two hours after transfection, the fluorescence intensity of the U87MG cells was observed via IVIS Spectrum system (PerkinElmer, Waltham, MA, USA).

BALB/c nude mice (6-week-old) were injected intracranially with U87 MG cells expressing firefly luciferase. After D-luciferin (10 µL/g; Beyotime) injection, the IVIS Spectrum system (PerkinElmer, Waltham, MA, USA) was used to capture the luminescence images. Ethical approval for animal experiments was granted by the Tianjin Medical University Institutional Animal Care Committee.

2.16. Statistical analysis

The collected clinical data were compiled using SPSS software (IBM, Chicago, IL, USA, version 20.0). Numeric data were expressed as the mean ± standard deviation (SD). Mean comparisons were performed using either Student's t-test or one-way analysis of variance. The Kaplan-Meier (KM) method was employed to evaluate patient survival. Based on median gene expression, all patients were stratified into two subgroups. Values of $P < 0.05$ were deemed statistically significant; *$P < 0.05$, **$P < 0.01$, ***$P < 0.001$ or ****$P < 0.0001$. All statistical plots were generated using GraphPad Prism (La Jolla, CA, USA, version 9.0.0). Each experiment involving cell lines was performed in triplicate.

3. Theory

In this study, we first identified an amplification in *APTR* in patients with gliomas and then confirmed the relationship between *APTR* gene copy amplification and patient survival. Our results revealed that APTR may serve as a potential prognostic biomarker for patients with gliomas. Further analysis indicated that APTR acts as a ceRNA that targets miR-6734-5p. By suppressing miR-6734-5p, APTR promotes the expression of TCF7 and LEF1 and induces the transcription of downstream CCND1 and MYC [13], thereby enhancing tumor cell migration, invasion, and proliferation. Our results indicate that *APTR* amplification leads to APTR overexpression and malignant progression of gliomas.

4. Results

4.1. APTR gene amplification and expression levels are correlated with glioma grade and patient prognosis

APTR gene copy amplification carried out for 153 WHO grade 2–4 glioma samples, including 41 grade 2 diffuse astrocytomas, 42 grade 3 anaplastic astrocytomas, and 70 GBMs, is shown in the left panel of Fig. 1A. *APTR* gene copy amplification for the TCGA GBM + LGG dataset is shown in the right panel of Fig. 1A. In both datasets, *APTR* gene copy amplification was correlated with glioma grade (Fig. 1A). The RNA expression levels of *APTR* in the TMUGH glioma samples showed that APTR was significantly increased in high-grade gliomas, and the level correlated with the glioma grade (Fig. 1B, left panel, $P < 0.0001$). Similarly, the RNA expression data from the TCGA database showed that the APTR expression level increased as the WHO grade increased (Fig. 1B, right panel, $P < 0.01$–0.001). Moreover, the copy number of *APTR* was positively correlated with APTR expression (Fig. 1C). Pan-cancer analysis showed distinct differences in APTR expression levels between normal and glioma tissues (GBM and LGG) from the TCGA

database (Fig. 1D). The above data indicate that the amplification of *APTR* copy number contributes to its overexpression, and both *APTR* amplification and APTR overexpression could predict a higher WHO glioma grade.

4.2. APTR gene amplification is associated with reduced survival durations in patients with gliomas

To evaluate the influence of APTR on the prognosis of patients with gliomas, KM survival analyses were conducted. Among the 153 glioma samples from TMUGH patients, those with *APTR* gene amplification had shorter overall survival (OS; Fig. 2A, left panel) and disease-free survival (DFS; Supplementary Fig. 1A, left panel). The above trends were confirmed in the TCGA dataset for LGG and GBM samples (Fig. 2A, right panel, Supplementary Fig. 1A, right panel). Grade 4 GBM samples were isolated from all patients with gliomas for further analysis. Similar results were observed in both the TMUGH grade 4 patients and the TCGA-GBM dataset, where *APTR* amplification was associated with a shorter OS (Fig. 2B) and DFS (Supplementary Fig. 1B). APTR expression levels were controlled by its copy number. The relationships between APTR level and patient survival were further assessed using the KM method. Elevated APTR expression correlated with reduced OS (Fig. 2C) and DFS (Supplementary Fig. 1C) in all grades from the TMUGH samples and TCGA datasets. Individually analyzed data of patients with GBM also showed similar results (Fig. 2D, Supplementary Fig. 1D).

Receiver operating characteristic (ROC) curves were calculated to assess the specificity of *APTR* copy number and expression for the survival status of patients with gliomas. In glioma samples of all grades, the area under the curve (AUC) for *APTR* copy number in OS was 81.20 % (Fig. 2E, left panel, WHO grade 2–4 glioma, $P < 0.0001$) and 71.69 % (Fig. 2E, right panel, TCGA LGG + GBM, $P < 0.0001$). For DFS, the AUCs for *APTR* copy number were 89.66 % (Supplementary Fig. 1E left panel, WHO grade 2–4 glioma, $P < 0.01$) and 70.05 % (Supplementary Fig. 1E
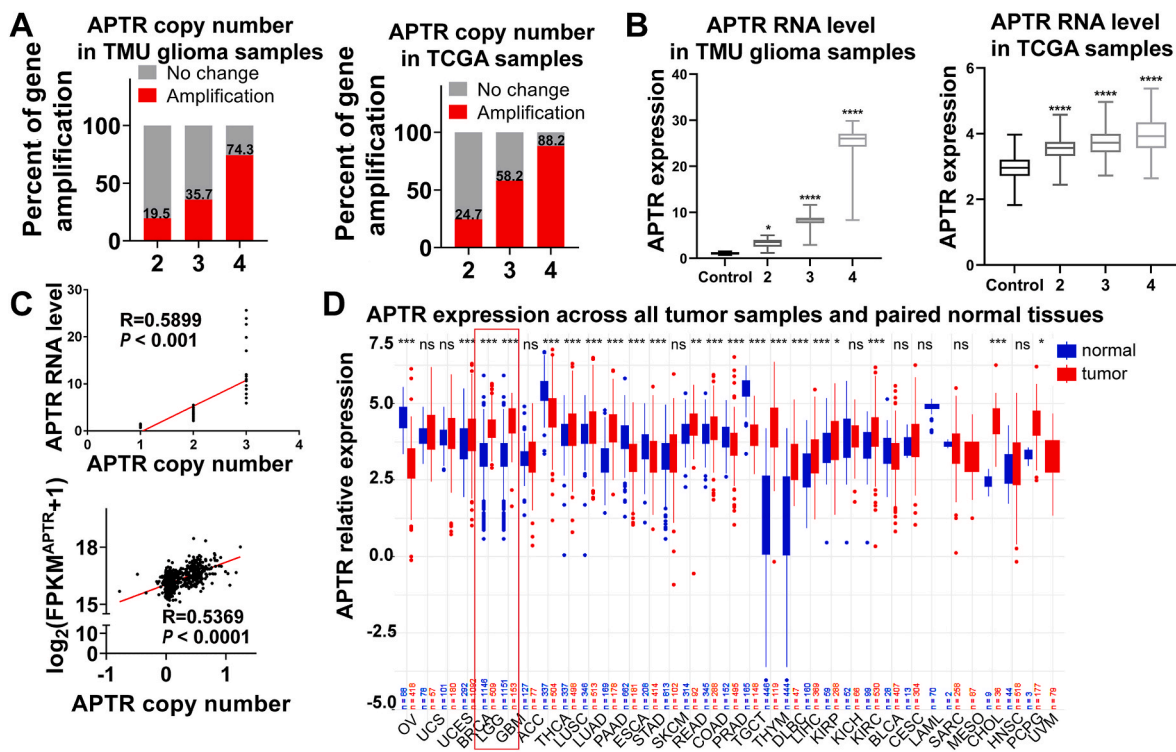
Fig. 1. APTR levels are associated with WHO grades of glioma. **(A)** *APTR* gene amplification rate in WHO grade 2–4 glioma samples from TMUGH samples (left panel, n = 153) and TCGA datasets (right panel, n = 603). **(B)** The expression level of *APTR* between different grades of glioma from TMUGH samples (left, control = 20) and TCGA datasets (right, control = 105). **(C)** *APTR* copy number is positively correlated with its expression level in TMUGH samples (upper panel) and TCGA datasets (lower panel). **(D)** The pan-cancer atlas depicting APTR expression in multiple tissues. *$P < 0.05$; ***$P < 0.001$; ****$P < 0.0001$.
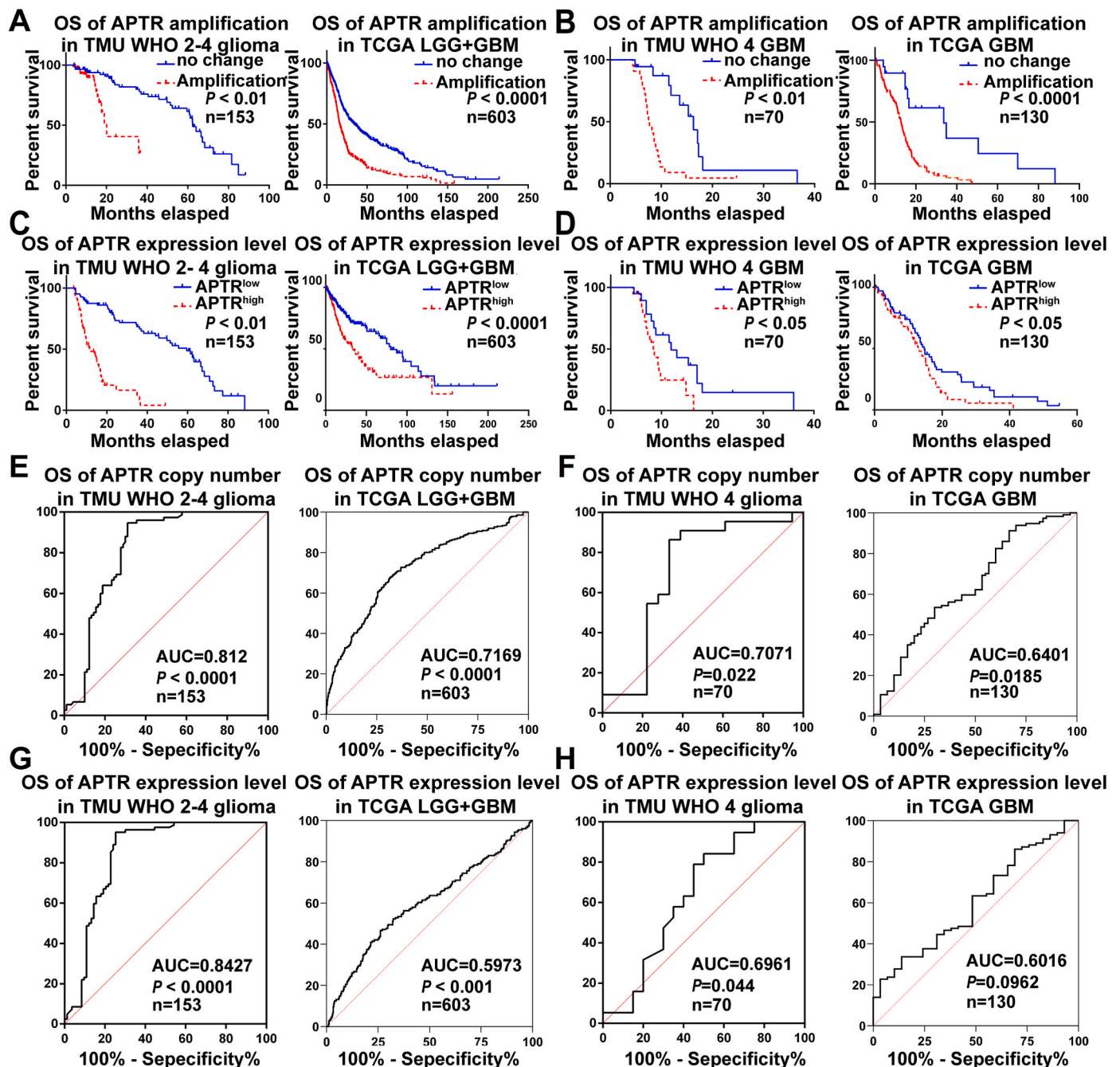
Fig. 2. *APTR* amplification pattern and expression level as a prognostic biomarker for glioma. **(A)** Kaplan-Meier (KM) analysis of overall survival (OS) time in WHO grade 2–4 gliomas from TMUGH samples (left, n = 153) and LGG + GBM samples from the TCGA dataset (right, n = 603) with samples stratified by *APTR* amplification status. **(B)** KM analysis of OS in WHO grade 4 gliomas from TMUGH samples (left, n = 70) and GBM samples from the TCGA dataset (right, n = 130) with samples stratified by *APTR* amplification status; **(C)** KM results revealed the OS outcome in WHO grade 2–4 gliomas from TMUGH samples (left, n = 153) and LGG and GBM samples from the TCGA dataset (right, n = 603) with samples stratified by APTR expression level. **(D)** KM was applied to assess OS in the WHO grade 4 gliomas from TMUGH samples (left, n = 70) and LGG + GBM samples from the TCGA dataset (right, n = 130) with samples stratified by APTR expression level. **(E–F)** Receiver operating characteristic (ROC) curve to illustrated relationships between OS and *APTR* amplification status in grade 2–4 gliomas from TMUGH samples (left) and the TCGA LGG + GBM datasets (right). **(G–H)** An ROC curve was used to plot the correlation between OS and RNA expression level in grade 2–4 gliomas from TMUGH samples (left) and the TCGA LGG + GBM datasets (right).

right panel, TCGA LGG + GBM, $P < 0.0001$). For grade 4 GBM samples, the AUCs for OS were 70.71 % (Fig. 2F left panel, WHO grade 4 glioma, $P = 0.022$) and 64.01 % (Fig. 2F right panel, TCGA GBM, $P = 0.0185$). The AUCs for DFS were 70.83 % (Supplementary Fig. 1F left panel, WHO grade 4 glioma, $P < 0.024$) and 67.66 % (Supplementary Fig. 1F right panel, TCGA GBM, $P = 0.0170$). APTR expression showed a similar relationship with the survival status of patients with gliomas of all

grades (Fig. 2G, Supplementary Fig. 1G) and grade 4 GBM samples (Fig. 2H, Supplementary Fig. 1H).

Univariate and multivariate Cox regression analyses were used to investigate the clinical data of patients with gliomas. These results suggest that both *APTR* amplification and APTR overexpression could be used as independent risk factors for predicting patient survival (Fig. 3A, Supplementary Fig. 2A, Supplementary Tables 4–7). The same results
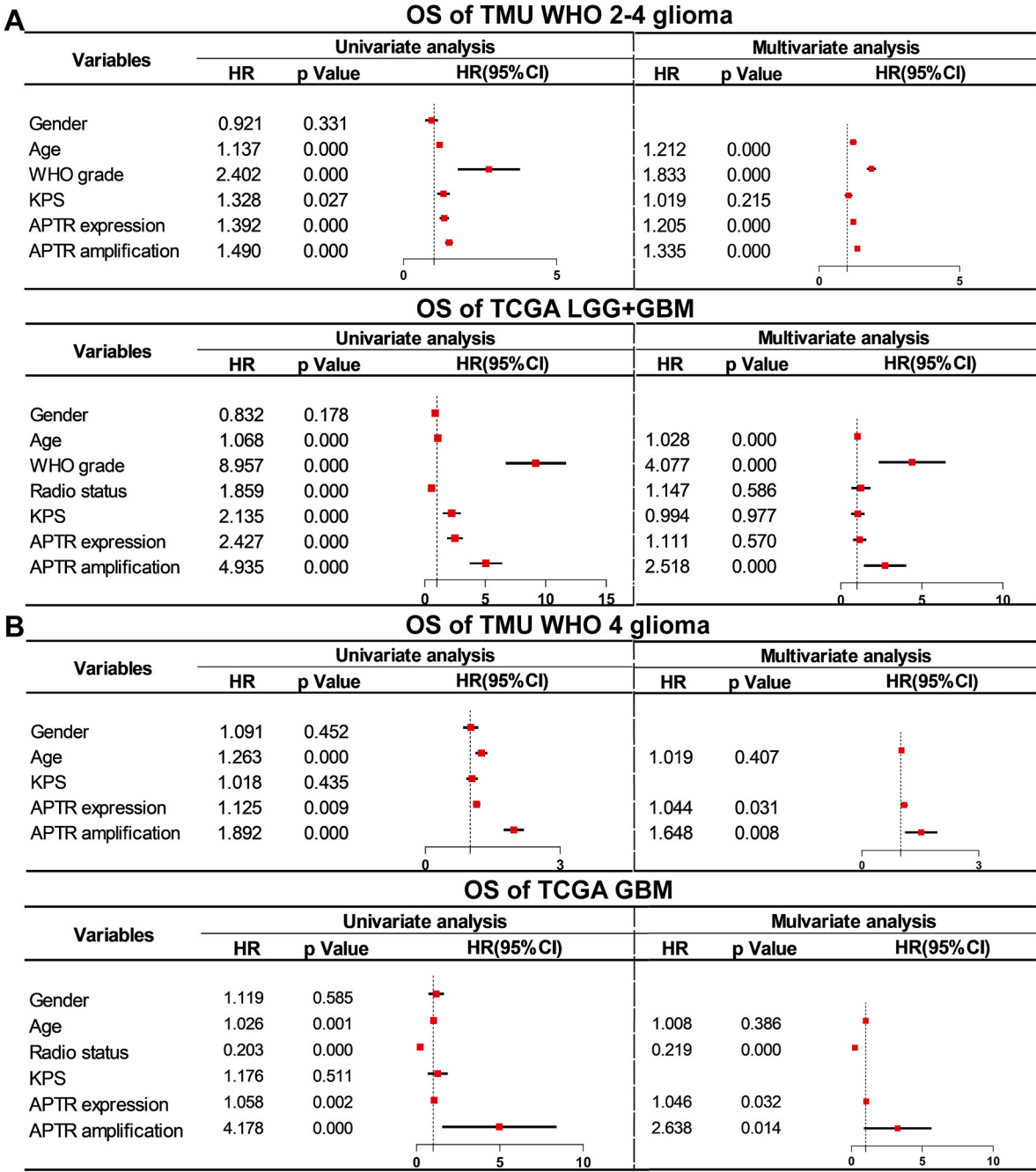
A

OS of TMU WHO 2-4 glioma

Variables	Univariate analysis			Multivariate analysis		
	HR	p Value	HR(95%CI)	HR	p Value	HR(95%CI)
Gender	0.921	0.331				
Age	1.137	0.000		1.212	0.000	
WHO grade	2.402	0.000		1.833	0.000	
KPS	1.328	0.027		1.019	0.215	
APTR expression	1.392	0.000		1.205	0.000	
APTR amplification	1.490	0.000		1.335	0.000	

OS of TCGA LGG+GBM

Variables	Univariate analysis			Multivariate analysis		
	HR	p Value	HR(95%CI)	HR	p Value	HR(95%CI)
Gender	0.832	0.178				
Age	1.068	0.000		1.028	0.000	
WHO grade	8.957	0.000		4.077	0.000	
Radio status	1.859	0.000		1.147	0.586	
KPS	2.135	0.000		0.994	0.977	
APTR expression	2.427	0.000		1.111	0.570	
APTR amplification	4.935	0.000		2.518	0.000	

B

OS of TMU WHO 4 glioma

Variables	Univariate analysis			Multivariate analysis		
	HR	p Value	HR(95%CI)	HR	p Value	HR(95%CI)
Gender	1.091	0.452				
Age	1.263	0.000		1.019	0.407	
KPS	1.018	0.435				
APTR expression	1.125	0.009		1.044	0.031	
APTR amplification	1.892	0.000		1.648	0.008	

OS of TCGA GBM

Variables	Univariate analysis			Mulvariate analysis		
	HR	p Value	HR(95%CI)	HR	p Value	HR(95%CI)
Gender	1.119	0.585				
Age	1.026	0.001		1.008	0.386	
Radio status	0.203	0.000		0.219	0.000	
KPS	1.176	0.511				
APTR expression	1.058	0.002		1.046	0.032	
APTR amplification	4.178	0.000		2.638	0.014	

Fig. 3. *APTR* amplification pattern and expression level as a prognostic biomarker for glioma. **(A)** The influence of *APTR* amplification status and RNA expression level on the OS in grade 2–4 gliomas from TMUGH samples (upper) and the TCGA LGG + GBM datasets (lower) displayed using a forest plot. **(B)** The impact of *APTR* amplification status and RNA expression levels on the OS in grade 4 gliomas from TMUGH samples (upper) and the TCGA GBM datasets (lower) was visualized using a forest plot.

were observed for GBM in both the TMUGH samples and TCGA datasets (Fig. 3B, Supplementary Fig. 2B, Supplementary Tables 8–11). These results support those of our previous study showing that copy number and expression of APTR were associated with the prognosis of patients with gliomas.

4.3. APTR promotes the malignancy of GBM cells

To examine the effects of APTR on GBM cell characteristics, stable APTR-knockdown U87MG and U251 cell lines were constructed, and CCK-8, colony formation, wound healing, and transwell assays were performed. qRT-PCR was performed to confirm the knockdown effect

(Fig. 4A). The CCK-8 assay and clone formation experiment showed that compared to control cells (Scramble), proliferation ability was suppressed in APTR knockdown cells (APTR-sh1/2, Fig. 4B and C). Additionally, after APTR knockdown, cell migration (Fig. 4D) and invasion (Fig. 4E) were significantly attenuated. We investigated the effects of APTR on GBM *in vivo*. The U87MG Scramble, U87MG APTR-sh1, and U87MG APTR-sh2 cells were infected with a lentivirus carrying firefly luciferase. These cells were intracranially implanted in 6-week-old BALB/c nude mice (n = 5). Bioluminescence imaging showed that mice injected with APTR-knockdown cells bore smaller tumors than those in the control group (Fig. 4F). The survival time of mice bearing APTR-knockdown cells was also significantly longer than that of mice in
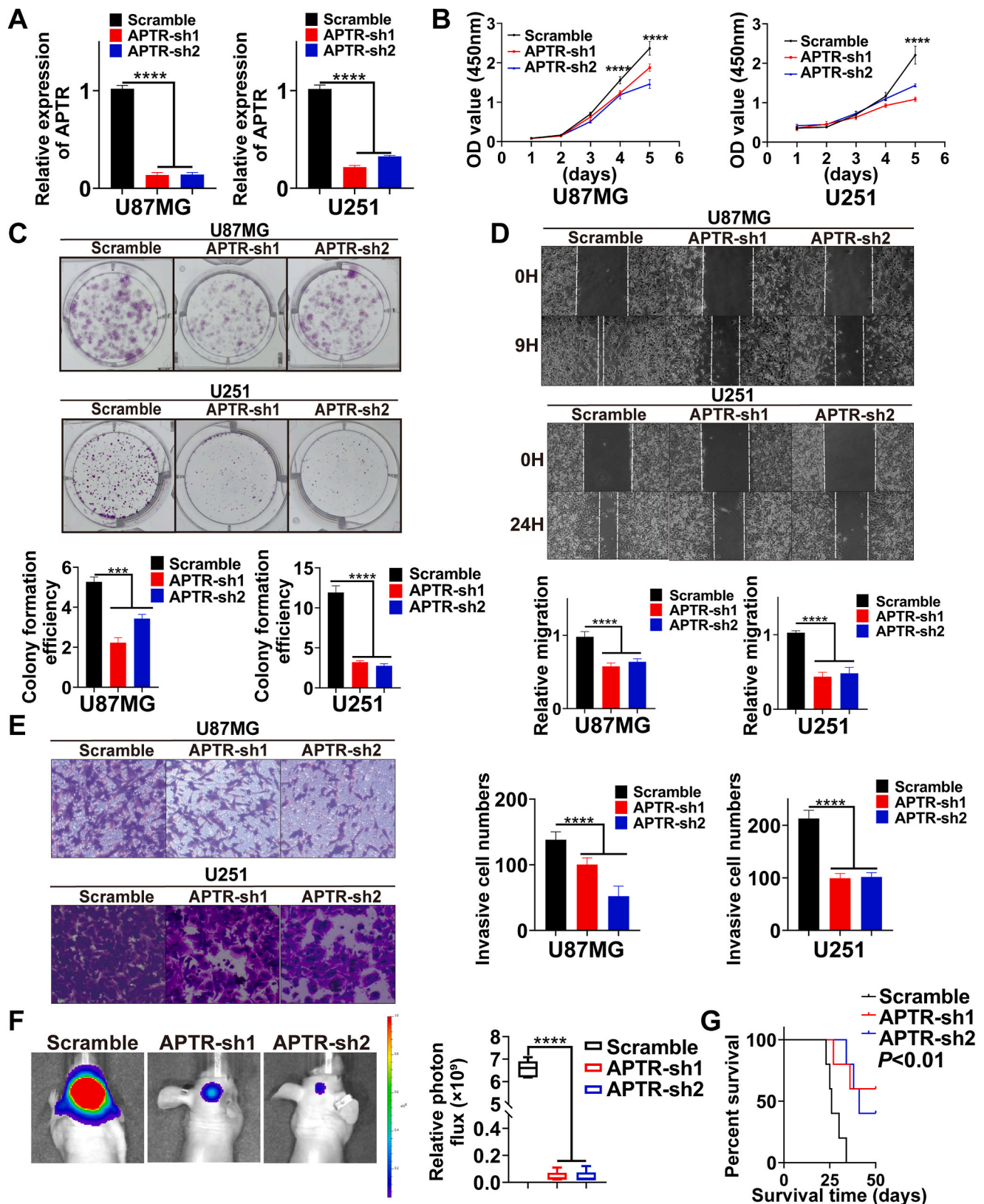
Fig. 4. APTR knockdown inhibits the malignant phenotype of GBM cells *in vivo* and *in vitro*. **(A)** qRT-PCR results confirmed APTR knockdown in U87MG and U251 cells (n = 3). **(B)** Cell Counting Kit-8 assays assessed GBM cell proliferation after APTR knockdown (n = 3). **(C)** Representative graphs and statistical results of cell clone formation experiments (n = 3). **(D)** Wound-healing assays assessed GBM cell migration capacity after APTR knockdown (n = 3). **(E)** Transwell assays assessed GBM cell invasion ability after APTR knockdown (n = 3). **(F)** Representative bioluminescent images of xenograft tumors with the corresponding quantitative analyses obtained from BALB/c nude mice in the U87MG control group (Scramble) and shAPTR groups (APTR-sh1 and APTR-sh2) (n = 5). **(G)** Survival curves for glioma-bearing mice in the control group (Scramble) and APTR knockdown groups (APTR-sh1 and APTR-sh2) under the indicated conditions (n = 5). ****$P < 0.0001$. Data are expressed as the mean ± SD.

the control group (Fig. 4G, $P < 0.01$). These results indicate that APTR enhanced the malignant phenotype of GBM cells.

4.4. APTR acts as a sponge for miR-6734-5p

To uncover the potential molecular mechanism of action of APTR, we initially performed a fluorescence *in situ* hybridization (FISH) assay in U87MG and U251 cells, which revealed that APTR exhibits cytoplasmic predominance (Fig. 5A). Subsequently, nucleoplasmic separation experiments validated that although a small amount of APTR was present in the nucleus, it was mostly located in the cytoplasm (Fig. 5B). We hypothesized that APTR acts as a molecular sponge for the adsorption of
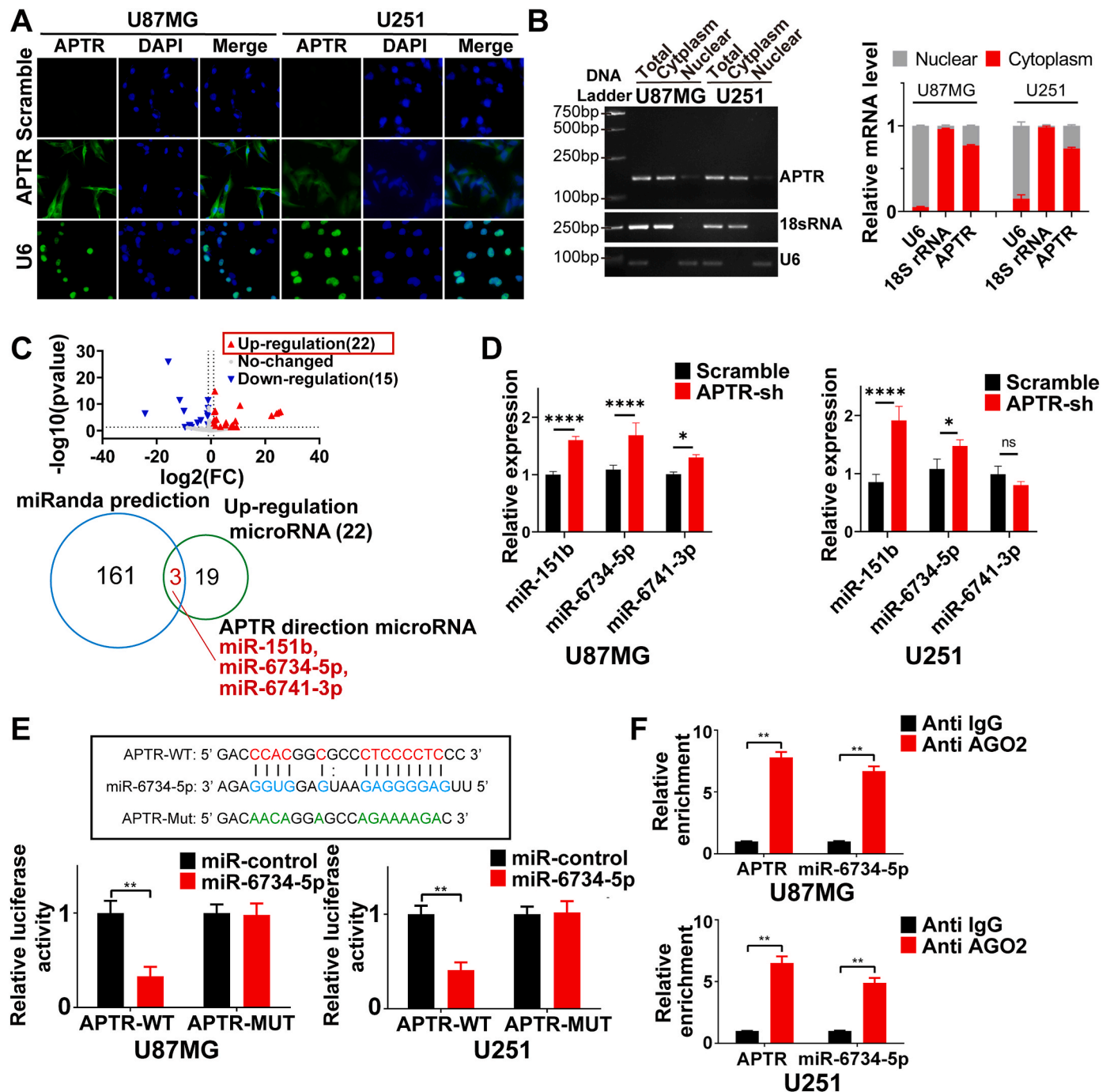

Fig. 5. APTR functions as a sponge for miR-6734-5p. **(A)** FISH was performed to visualize the intracellular localization of APTR (green), Scramble probe served as negative control, U6 probe served as positive control. **(B)** Nuclear-cytoplasmic separation of RNA from U87MG and U251 cells was followed by RT-PCR amplification, and the results were detected using agarose gel electrophoresis. **(C)** Volcano plots showing the differentially expressed microRNA (miRNA) after APTR knockdown (upper). The intersection between the up-regulated miRNAs (n = 22) from miRNA-seq and the miRNAs predicted by miRanda (n = 164) was determined to identify miRNAs that potentially bind to APTR (lower). **(D)** qRT-PCR results showing the miRNA expression levels in U87MG and U251 cells with APTR knockdown. **(E)** Schematic representation of the luciferase reporter plasmids, including one with the APTR interaction miRNA sequence and another without (upper panel). The dual luciferase reporter assay verified the targeting relationship between APTR and miR-6734-5p (lower panel). **(F)** An Anti-AGO2 RIP assay was performed in U87MG and U251 cells, followed by qRT-PCR to detect the enrichment ability of AGO2 on APTR or miR-6734-5p compared to that of IgG. $*P < 0.05$; $**P < 0.01$; $****P < 0.0001$.

miRNAs. To elucidate the molecular mechanisms underlying APTR function, RNA-sequencing (RNA-seq) was used to screen for miRNAs that were altered after APTR knockdown. We screened 22 miRNA candidates that were upregulated after APTR knockdown (Fig. 5C, upper panel, Supplementary Table 12). We used the miRNA target prediction software miRanda to predict potential APTR targets and identified 164 potential APTR-binding targets (Supplementary Table 13). By overlapping these two sets, we identified three highly reliable miRNAs (Fig. 5C, lower panel). qRT-PCR validation revealed that miR-151b and miR-6734-5p were markedly upregulated in both U87MG and U251 knockdown cell lines (APTR-sh, Fig. 5D). The above prediction analysis was validated using dual-luciferase reporter and RIP assays. Two variant *APTR* sequences, one with wild-type and the other with mutated miR-151b and miR-6734-5p binding sequences were inserted separately into the dual-luciferase reporter plasmid pmirGLO (Fig. 5E, Supplementary Fig. 3A). Only luciferase activity in the wild-type group (APTR-WT, $P < 0.001$) was markedly reduced by the miR-6734-5p mimic compared to the miR-NC transfection, while the luminance signal of the mutation group was not inhibited (APTR-MUT, Fig. 5E). The miR-151b had no interaction with APTR (Supplementary Fig. 3A). We observed obvious upregulation of APTR and miR-6734-5p in cells treated with the AGO2 protein, a key component of the RNA-induced silencing complex (RISC), in contrast to that using the negative control IgG (Fig. 5F). These results suggested that APTR directly interacts with miR-6734-5p.

4.5. APTR induces Wnt signaling via miR-6734-5p

To identify the gene transcription alterations after APTR-induced attenuation of miR-6734-5p, we performed RNA-seq to detect differentially expressed genes after APTR knockdown. The candidate genes sharing a 3′UTR sequence with miR-6734-5p were collected and analyzed (Fig. 6A). We screened 1098 transcripts that were downregulated after APTR knockdown using differential gene analysis (fold change >2, q < 0.05), which included 867 protein-coding genes (Supplementary Table 14). The functions of the candidate genes were clustered using Kyoto Encyclopedia of Genes and Genomes (KEGG) analysis (Fig. 6B–Supplementary Table 15). Targetscan (https://www.targetscan.org/vert_80/) was used to forecast potential interactions between the transcript and the 3′UTR of miRNA. Next, 3888 target genes of miR-6734-5p were screened (Supplementary Table 16). A total of 170 genes were identified by overlapping the above sets (Fig. 6C–Supplementary Table 17). Gene Ontology (GO) analysis (Supplementary Table 18) showed that APTR/miR-6734-5p is associated with the Wnt signaling pathway and focal adhesion (Fig. 6D). The differentially expressed genes involved in the Wnt signaling pathway included *TCF7, LEF1, WNT5A, DDIT3, TNIK, WWOX,* and *CDC73.*

The Wnt pathway-mediated genes, *TCF7* and *LEF1,* were then were selected as targets. The RNA expression data from the TCGA database showed that the expression levels of *TCF7* and *LEF1* increased with an increase in WHO glioma grade (Fig. 6E). Moreover, patients with higher TCF7/LEF1 expression levels had a shorter survival time in LGG + GBM samples from TCGA database (Supplementary Figs. 4A–D). IHC was used to detect TCF7 and LEF1 in paraffin-embedded specimens from 153 cases of gliomas of different WHO grades and 20 control brain tissue samples (Supplementary Table 1). The results showed that the expression of TCF7 and LEF1 significantly increased in high-grade gliomas (Fig. 6F and G, Supplementary Tables 12–13). In addition, TCF7 and LEF1 levels in 70 GBM tissue samples form TMUGH were negatively correlated with miR-6734-5p expression (Fig. 6H, $P < 0.001$).

4.6. APTR induces Wnt signaling by promoting TCF7/LEF1 expression

The expression of TCF7 and LEF1 in U87MG and U251 cells was detected using qRT-PCR and western blotting. The results showed that the mRNA and protein expression of both TCF7 and LEF1 decreased after APTR knockdown in the GBM cell lines (Fig. 7A and B). The above cells

were transfected with a luciferase reporter vector containing a conserved TCF/LEF1 binding sequence, and the luciferase signals were significantly decreased in APTR-knockdown cells (APTR sh1/2) compared with those in control cells (Scramble, Fig. 7C). Western blotting results showed that the levels of CCND1 and c-MYC, well-documented downstream targets of TCF7/LEF1, were also decreased in APTR-knockdown cells (Fig. 7B, APTR sh1/2 CCND1 and c-MYC). As targets of APTR, miR-6734-5p mimics also suppressed the expression of TCF7 and LEF1 at both the mRNA and protein levels (Fig. 7D and E). Moreover, c-MYC and CCND1 levels were decreased in miR-6734-5p mimic-transfected cells due to the deficiency of TCF/LEF1 (Fig. 7E, miR-6734-5p mimics CCND1 and c-MYC). These results suggest that the inhibition of TCF and LEF1 gene expression induced by APTR knockdown might be mediated by miR-6734-5p. The luciferase reporter assay showed that compared to the control group (miR-control), the relative luciferase activity was reduced upon transfection with miR-6734-5p mimics (miR-6734-5p, Fig. 7F). The 3′UTR of TCF7 and LEF1 was shown to harbor direct miR-6734-5p binding sites (Fig. 7G and H, upper panel). The dual-luciferase reporter assay showed that miR-6734-5p mimics significantly decreased the activity of a luciferase reporter vector carrying the TCF7/LEF1 3′UTR-WT sequence (TCF7/LEF1-WT) but not that of the mutant sequence group (TCF7/LEF1-MUT; Fig. 7G and H, middle and lower panel). The interaction between miR-6734-5p and TCF7/LEF1 was validated using an AGO2-RIP assay (Fig. 7I). These results showed that APTR modulates the expression of TCF7 and LEF1 in GBM through its role as a ceRNA for miR-6734-5p.

4.7. APTR promotes a malignant GBM cell phenotype through the APTR/miR-6734-5p/TCF7/LEF1 axis

To investigate whether the APTR/miR-6734-5p/TCF7/LEF1 axis contributes to the malignant GBM cell phenotype, we used miR-6734-5p-specific antisense oligonucleotide molecule (ASO) for rescue experiments. Western blot analysis revealed that the protein levels of TCF7, LEF1, CCND1, and c-Myc were restored by miR-6734-5p-specific ASO transfection (Fig. 8A). Moreover, the relative luciferase activity was also recovered (Fig. 8B). Phenotype experiments indicated that after miR-6734-5p-specific ASO transfection, the proliferation, invasion and migration-inhibiting functions triggered by APTR knockdown were recovered in U87MG and U251 cells (Fig. 8C–E, Supplementary Figs. 5A–D). In conclusion, the above results demonstrate that APTR, which functions as a ceRNA of miR-6734-5p, modulates TCF7 and LEF1 expression, thereby promoting the proliferation, migration, and invasion of GBM cells (Fig. 8F).

5. Discussion

In this study, we identified *APTR* copy amplification in glioma samples. APTR expression levels in glioma samples were positively correlated with *APTR* amplification patterns. In glioma samples from TMUGH and the TCGA datasets, *APTR* amplification and expression levels were increased in higher-grade gliomas and were highest in GBM. Moreover, multivariate and univariate COX analyses revealed that *APTR* amplification and expression may serve as novel prognostic factors for individual gliomas.

APTR is ubiquitously expressed in the thyroid, testis, brain, and other tissues. The APTR has two complementary Alu elements (c-Alu) and a complementary L2 element. It has been reported that, via the c-Alu element, APTR recruits PRC2 to the p21 gene promoter and inhibits its gene transcription [9]. APTR also interacts with ERs in the nucleus [10]. However, increasing evidence suggests that APTR may also act as ceRNAs in the cytoplasm [11,17]. Our data demonstrate cell-type specific subcellular localization patterns of *APTR*. *APTR* may be enriched in the nucleus by interactions with transcription factors such as ERα, otherwise it might remain in the cytoplasm. To confirm the hypothesis, FISH and RNA separation were performed in ERα-negative U87MG and U251
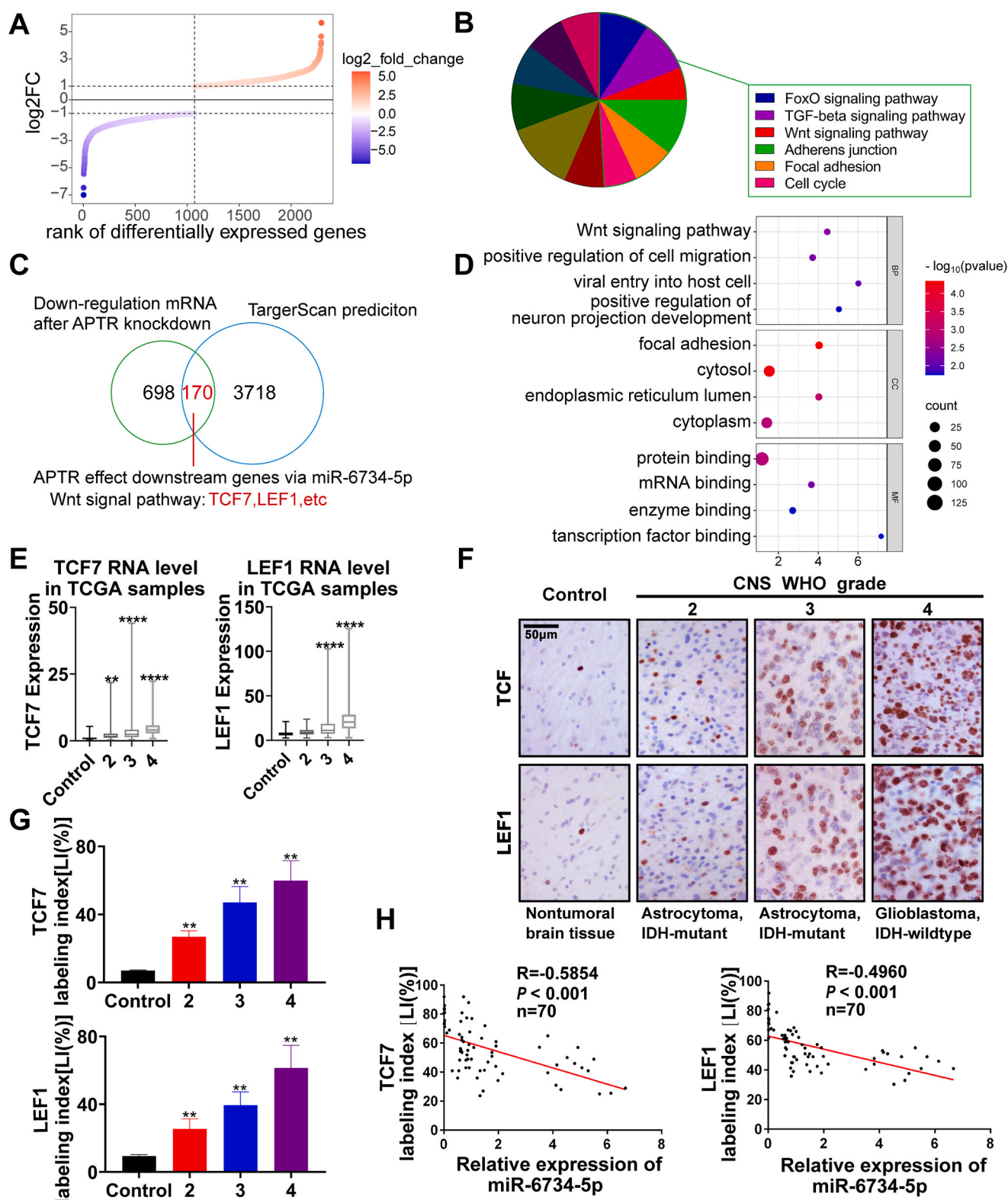
Fig. 6. APTR functions as a sponge for miR-6734-5p to modulate the Wnt signaling pathway. **(A)** Continuous scatter plot showed differential transcripts after APTR knockdown from RNA-seq. **(B)** Kyoto Encyclopedia of Genes and Genomes (KEGG) pathway enrichment analysis showing differential transcripts after APTR knockdown. **(C)** The overlap between downregulated genes identified in RNA-seq (868) and genes predicted by TargetScan (3888) to potentially bind with miR-6734-5p. **(D)** Bubble chart showing the Gene Ontology (GO) term enrichment analysis of the overlapped genes (n = 170). **(E)** The expression levels of TCF7 and LEF1 in gliomas of various grades from the TCGA database. **(F–G)** IHC staining of TCF7 and LEF1 (F). Protein levels (LI %) of TCF7 and LEF1 in 153 glioma samples and 20 control brain samples (G). Scale bar, 50 μm .**(H)** The relationship between miR-6734-5p and TCF7/LEF1 expression in GBM tissues analyzed using correlation coefficients. **$P < 0.01$; ***$P < 0.0001$.
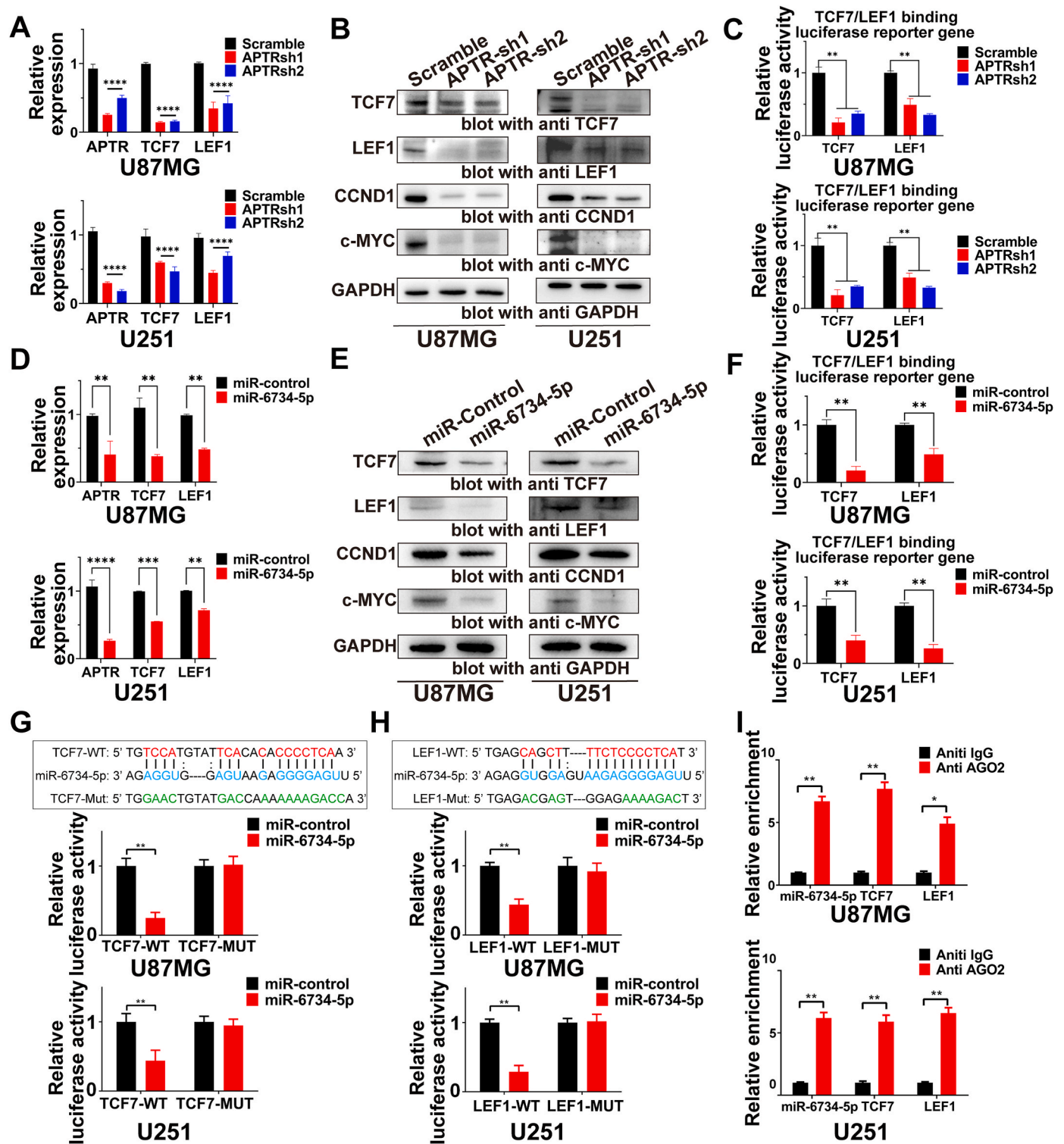
Fig. 7. APTR indirectly regulates miR-6734-5p that directly targets TCF7 and LEF1. (A–B) qRT-PCR analysis of the relative mRNA levels of *TCF7* and *LEF1* (A) and western blots showing the protein levels of TCF7, LEF1, MYC, and CCND1 (B) after APTR knockdown. (C) Luciferase activity quantified in GBM cells including control and APTR knockdown groups. (D–E) The relative mRNA expression of *TCF7* and *LEF1* was detected using qRT-PCR (D), while the protein levels of TCF7, LEF1, MYC, and CCND1 were determined using western blotting after transfection with miR-6734-5p mimics (E). (F) Luciferase activity was assessed in U87MG and U251 cells after transfection with miR-6734-5p mimics and TCF7/LEF1-binding reporter plasmids. (G) Schematic representation of the luciferase reporter plasmids, including TCF7 with (TCF7-WT) and without (TCF7-Mut) the miRNA interaction sequence (upper); luciferase activities were measured following transfection with TCF7-WT or TCF7-MUT and miR-6734-5p mimics or mimic-control in U87MG and U251 cells (lower). (H) Schematic illustration of the LEF1-WT and LEF1-MUT luciferase reporter vectors (upper panel). Relative luciferase activity in U87MG and U251 cells after transfection with the aforementioned plasmids and miR-6734-5p mimics or mimic-control (lower). (I) AGO2-RIP analysis verified the interaction between miR-6734-5p and TCF7/LEF1. *P < 0.05; **P < 0.01; ***P < 0.001; ****P < 0.0001.
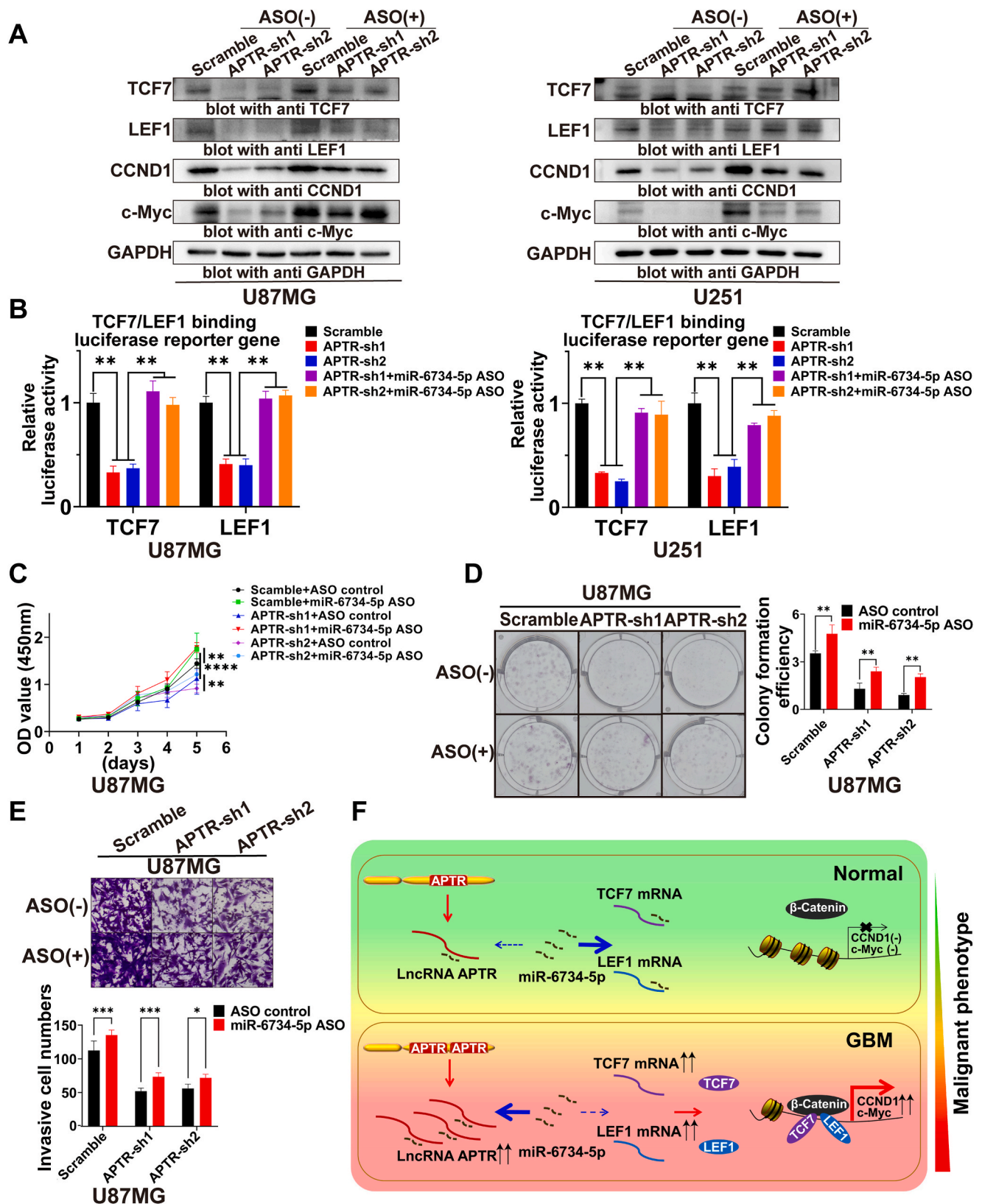
Fig. 8. APTR promotes malignant GBM cell phenotype through APTR/miR-6734-5p/TCF7/LEF1 axis. **(A)** Western blot results showing the protein levels of TCF7, LEF1, MYC, and CCND1 in U87MG and U251 cells after treatment with miR-6734-5p-specific ASO. **(B)** Relative luciferase activity measured in GBM cells after co-treatment with miR-6734-5p-specific ASO and TCF7/LEF1-binding reporter plasmids. **(C–E)** The cell proliferation (C, D) and invasion (E) were determined upon application of miR-6734-5p-specific ASO (n = 3). **(F)** Schematic diagram shows the mechanism underlying the promotion of malignant GBM cell phenotype by APTR. *$P < 0.05$; **$P < 0.01$; ***$P < 0.001$; ****$P < 0.0001$. Data are presented as mean ± SD.

cells. The results showed that APTR exhibits with cytoplasmic predominance. Based on the potential ceRNA function of APTR, further RIP and luciferase assays verified the interaction between APTR and miR-6734-5p.

Previous data have shown that miR-6734-5p regulates the development of colon cancer, bladder cancer, and acute myeloid leukemia [18–20]; however, the role of miR-6734-5p in glioma remains largely unknown. Dual-luciferase reporter and RIP assays indicated miR-6734-5p could also bind to the 3′UTR of TCF7/LEF1 mRNAs, these data indicated a novel function of miR-6734-5p, which may act as a bridge molecule between APTR and TCF7/LEF1.

The abnormal activation of canonical Wnt pathway induces malignant progression in various tumors [21–24]. TCF7 and LEF1 are the key mediators of Wnt signaling [25]. APTR knockdown significantly decreased the expression of TCF7 and LEF1 in GBM cell lines. Moreover, degradation of TCF7 and LEF1 further blocked Wnt signaling and repressed the transcription of CCND1 and MYC. Mechanistically; our results are the first to link *APTR* amplification with activation of the Wnt pathway in glioma.

In summary, we identified *APTR* amplification as a novel subclassification biomarker and potential prognostic predictor in patients with gliomas. Mechanistically, APTR acts as a ceRNA targeting miR-6734-5p, upregulates TCF7 and LEF1 expression, and promotes the malignant progression of glioma.

6. Conclusion

Our findings indicate that *APTR* amplification correlates with the WHO grade and prognosis of patients with gliomas. Thus, it has the potential to be a prognostic biomarker and glioma classification indicator. We discovered novel mechanisms of APTR in the glioma cytoplasm that drive the malignant progression of tumor cells. APTR plays the role of a "molecular sponge" by adsorbing miR-6734-5p, thereby affecting the expression of TCF7 and LEF1.

CRediT authorship contribution statement

Heng Chen: Data curation. **Mengzhen Huang:** Data curation. **Jiayi Li:** Methodology, Data curation. **Shanshan Zhang:** Resources, Project administration, Methodology. **Cuiyun Sun:** Visualization, Software, Methodology. **Wenjun Luo:** Validation, Software, Methodology. **Lin Yu:** Writing – review & editing, Supervision, Funding acquisition, Conceptualization.

Ethics approval and consent to participate

All the data adhered to the principles stated in the Declaration of Helsinki and conformed to the ethical guidelines set forth by the TMU Ethics Committee. The ethics approval numbers for the analysis of clinical samples and the animal experiment are IRB2020-KY-289 and TMUaMEC2023012.

Consent for publication

All persons have granted their consent for publication.

Availability of data and materials

All data generated and investigated throughout this research has been incorporated into this published article along with its supplementary documentation.

Funding

Declaration of competing interest

The authors declare that they have no known competing financial interests or personal relationships that could have appeared to influence the work reported in this paper.

Appendix A. Supplementary data

Supplementary data to this article can be found online at https://doi.org/10.1016/j.ncrna.2025.02.007.

References

[1] D. Xiao, C. Yan, D. Li, T. Xi, X. Liu, D. Zhu, G. Huang, J. Xu, Z. He, A. Wu, C. Ma, J. Long, K. Shu, H. Ji, N. Wang, G. Chen, J. Yang, H. Ma, Z. Li, X. Sun, Y. Qu, Z. Liu, X. Jiang, C. Tian, S. Ni, R. Zhan, L. Chen, M. Ge, M. Wang, X. Jiang, G. Guo, Z. Han, C. Zhang, T. Zhang, C. Dou, L. Chu, P. Wang, J. Shao, X. Wu, J. Yu, Y. Wang, N. Wu, R. Zhang, M. Zhang, Y. Hong, J. Gao, Y. Li, Y. Pan, B. Zhao, N. Ji, G. Shan, C. B. Patel, W. Jia, L. Zhang, National Brain Tumour Registry of China (NBTRC) statistical report of primary brain tumours diagnosed in China in years 2019-2020, Lancet Reg. Health West Pac. 34 (2023) 100715, https://doi.org/10.1016/j.lanwpc.2023.100715.
[2] F. Chen, M.C. Wendl, M.A. Wyczalkowski, M.H. Bailey, Y. Li, L. Ding, Moving pan-cancer studies from basic research toward the clinic, Nat. Cancer 2 (2021) 879–890, https://doi.org/10.1038/s43018-021-00250-4.
[3] R. Stupp, S. Taillibert, A. Kanner, W. Read, D. Steinberg, B. Lhermitte, S. Toms, A. Idbaih, M.S. Ahluwalia, K. Fink, F. Di Meco, F. Lieberman, J.J. Zhu, G. Stragliotto, D. Tran, S. Brem, A. Hottinger, E.D. Kirson, G. Lavy-Shahaf, U. Weinberg, C.Y. Kim, S.H. Paek, G. Nicholas, J. Bruna, H. Hirte, M. Weller, Y. Palti, M.E. Hegi, Z. Ram, Effect of tumor-treating fields plus maintenance temozolomide vs maintenance temozolomide alone on survival in patients with glioblastoma: a randomized clinical trial, JAMA 318 (2017) 2306–2316, https://doi.org/10.1001/jama.2017.18718.
[4] N.E. Synhaeve, M.J. van den Bent, P.J. French, W.N.M. Dinjens, P.N. Atmodimedjo, J.M. Kros, R. Verdijk, C.M.F. Dirven, H.J. Dubbink, Clinical evaluation of a dedicated next generation sequencing panel for routine glioma diagnostics, Acta Neuropathol. Commun. 6 (2018) 126, https://doi.org/10.1186/s40478-018-0633-y.
[5] G.Y. Lopez, J. Van Ziffle, C. Onodera, J.P. Grenert, I. Yeh, B.C. Bastian, J. Clarke, N. A. Oberheim Bush, J. Taylor, S. Chang, N. Butowski, A. Banerjee, S. Mueller, C. Kline, J. Torkildson, D. Samuel, A. Siongco, C. Raffel, N. Gupta, S. Kunwar, P. Mummaneni, M. Aghi, P. Theodosopoulos, M. Berger, J.J. Phillips, M. Pekmezci, T. Tihan, A.W. Bollen, A. Perry, D.A. Solomon, The genetic landscape of gliomas arising after therapeutic radiation, Acta Neuropathol. 137 (2019) 139–150, https://doi.org/10.1007/s00401-018-1906-z.
[6] L. Li, V.T. Puliyappadamba, S. Chakraborty, A. Rehman, V. Vemireddy, D. Saha, R. F. Souza, K.J. Hatanpaa, P. Koduru, S. Burma, D.A. Boothman, A.A. Habib, EGFR wild type antagonizes EGFRvIII-mediated activation of Met in glioblastoma, Oncogene 34 (2015) 129–134, https://doi.org/10.1038/onc.2013.534.
[7] S. Zhang, M. Gao, L. Yu, GATAD1 gene amplification promotes glioma malignancy by directly regulating CCND1 transcription, Cancer Med. 8 (2019) 5242–5253, https://doi.org/10.1002/cam4.2405.
[8] C.W. Brennan, R.G. Verhaak, A. McKenna, B. Campos, H. Noushmehr, S.R. Salama, S. Zheng, D. Chakravarty, J.Z. Sanborn, S.H. Berman, R. Beroukhim, B. Bernard, C. J. Wu, G. Genovese, I. Shmulevich, J. Barnholtz-Sloan, L. Zou, R. Vegesna, S. A. Shukla, G. Ciriello, W.K. Yung, W. Zhang, C. Sougnez, T. Mikkelsen, K. Aldape, D.D. Bigner, E.G. Van Meir, M. Prados, A. Sloan, K.L. Black, J. Eschbacher, G. Finocchiaro, W. Friedman, D.W. Andrews, A. Guha, M. Iacocca, B.P. O'Neill, G. Foltz, J. Myers, D.J. Weisenberger, R. Penny, R. Kucherlapati, C.M. Perou, D. N. Hayes, R. Gibbs, M. Marra, G.B. Mills, E. Lander, P. Spellman, R. Wilson, C. Sander, J. Weinstein, M. Meyerson, S. Gabriel, P.W. Laird, D. Haussler, G. Getz, L. Chin, Tcga Research Network, the somatic genomic landscape of glioblastoma, Cell 155 (2013) 462–477, https://doi.org/10.1016/j.cell.2013.09.034.
[9] M. Negishi, S.P. Wongpalee, S. Sarkar, J. Park, K.Y. Lee, Y. Shibata, B.J. Reon, R. Abounader, Y. Suzuki, S. Sugano, A. Dutta, A new lncRNA, APTR, associates with and represses the cdkn1a/p21 promoter by recruiting polycomb proteins, PLoS One 9 (2014) e95216, https://doi.org/10.1371/journal.pone.0095216.
[10] W. Zhou, G. Wang, B. Li, J. Qu, Y. Zhang, LncRNA APTR promotes uterine leiomyoma cell proliferation by targeting ERα to activate the wnt/β-catenin pathway, Front. Oncol. 11 (2021) 536346, https://doi.org/10.3389/fonc.2021.536346.
[11] H. Guan, G. Shang, Y. Cui, J. Liu, X. Sun, W. Cao, Y. Wang, Y. Li, Long noncoding RNA APTR contributes to osteosarcoma progression through repression of miR-132-3p and upregulation of yes-associated protein 1, J. Cell. Physiol. 234 (2019) 8998–9007, https://doi.org/10.1002/jcp.27572.
[12] S. Yu, S. Qi, Y. Jiang, J. Jiang, H. Wang, Q. Zhou, APTR is a prognostic marker in cirrhotic patients with portal hypertension during TIPS procedure, Gene 645 (2018) 30–33, https://doi.org/10.1016/j.gene.2017.12.040.
[13] A. Ren, Q. Li, Y. Guo, X. Cui, L. Wang, Y. Huo, H. Chen, H. Liu, H. Huang, Low expression of lncRNA APTR promotes gastric cancer progression, Transl Oncol 25 (2022) 101506, https://doi.org/10.1016/j.tranon.2022.101506.

[14] K. Zhang, C. Li, J. Liu, Z. Li, C. Ma, Down-regulation of APTR and it's diagnostic value in papillary and anaplastic thyroid cancer, Pathol. Oncol. Res. 26 (2020) 559–565, https://doi.org/10.1007/s12253-018-0561-y.

[15] Y. Zhang, X. Wang, Targeting the Wnt/β-catenin signaling pathway in cancer, J. Hematol. Oncol. 13 (2020) 165, https://doi.org/10.1186/s13045-020-00990-3.

[16] J. Schuijers, M. Mokry, P. Hatzis, E. Cuppen, H. Clevers, Wnt-induced transcriptional activation is exclusively mediated by TCF/LEF, EMBO J. 33 (2014) 146–156, https://doi.org/10.1002/embj.201385358.

[17] Q. Zhao, S. Xiong, H. Cai, X. He, X. Shi, Expression and significance of the long non-coding RNA APTR in the occurrence and development of lung adenocarcinoma, J. Environ. Pathol. Toxicol. Oncol. 44 (2025) 11–20, https://doi.org/10.1615/JEnvironPatholToxicolOncol.2024053394.

[18] M.R. Kang, K.H. Park, J.-O. Yang, C.W. Lee, S.J. Oh, J. Yun, M.Y. Lee, S.-B. Han, J. S. Kang, miR-6734 up-regulates p21 gene expression and induces cell cycle arrest and apoptosis in colon cancer cells, PLoS One 11 (2016) e0160961, https://doi.org/10.1371/journal.pone.0160961.

[19] X. Hu, S. Xu, Y. Chen, Z. Gao, Y. Li, J. Hu, X. Huang, Y. Zhang, X. Jiang, L. Li, C. Yang, J. Chen, N. Gao, Depletion of Ars2 inhibits cell proliferation and leukemogenesis in acute myeloid leukemia by modulating the miR-6734-3p/p27 axis, Leukemia 33 (2019) 1090–1101, https://doi.org/10.1038/s41375-018-0301-z.

[20] Y. Wang, T. Yang, Y. Han, Z. Ren, J. Zou, J. Liu, S. Xi, lncRNA OTUD6B-AS1 exacerbates As2O3-induced oxidative damage in bladder cancer via miR-6734-5p-mediated functional inhibition of IDH2, Oxid. Med. Cell. Longev. 2020 (2020) 3035624, https://doi.org/10.1155/2020/3035624.

[21] Y.X. Lou, J. Gu, L. Zhu, S.Q. Sun, X.L. Hao, J.P. Chen, F. Han, D.D. Wang, X. Jiang, J.Y. Liu, TC2N promotes cell proliferation and metastasis in hepatocellular carcinoma by targeting the wnt/beta-catenin signaling pathway, Lab. Invest. 103 (2023) 100260, https://doi.org/10.1016/j.labinv.2023.100260.

[22] L. Zhu, Q. Tian, H. Gao, K. Wu, B. Wang, G. Ge, S. Jiang, K. Wang, C. Zhou, J. He, P. Liu, Y. Ren, B. Wang, PROX1 promotes breast cancer invasion and metastasis through WNT/beta-catenin pathway via interacting with hnRNPK, Int. J. Biol. Sci. 18 (2022) 2032–2046, https://doi.org/10.7150/ijbs.68960.

[23] M. Hemmati-Dinarvand, H. Ahmadvand, A. Seghatoleslam, Nitazoxanide and cancer drug resistance: targeting wnt/beta-catenin signaling pathway, Arch. Med. Res. 53 (2022) 263–270, https://doi.org/10.1016/j.arcmed.2021.12.001.

[24] J. Wang, H. Yu, W. Dong, C. Zhang, M. Hu, W. Ma, X. Jiang, H. Li, P. Yang, D. Xiang, N6-Methyladenosine-Mediated up-regulation of FZD10 regulates liver cancer stem cells' properties and lenvatinib resistance through WNT/beta-Catenin and hippo signaling pathways, Gastroenterology 164 (2023) 990–1005, https://doi.org/10.1053/j.gastro.2023.01.041.

[25] H. Clevers, Wnt/beta-catenin signaling in development and disease, Cell 127 (2006) 469–480, https://doi.org/10.1016/j.cell.2006.10.018.